第 43 卷 第 13 期/2023 年 7 月/光学学报 研究论文

光学学报

偏振复用CO-OFDM-OQAM系统的高频谱效率频域信道估计方法

张硕，王道斌*，赵航宇，黄全盛，宋婷婷，元丽华

兰州理工大学理学院，甘肃 兰州 730050

摘要 研究对象是偏移正交幅度调制的相干光正交频分复用通信(CO-OFDM-OQAM)系统的信道估计方法。为了减少训练序列所占用的频谱资源，进一步提升频谱效率，为偏振复用CO-OFDM-OQAM系统提出了一种新的频域信道估计方法。该方法利用偏振复用系统的解调原理和固有虚部干扰系数的对称性规律设计全负载型实值导频方案，结合插值法，将每个偏振态上训练序列需要占用的频域符号个数降低为4。此外，该方法的另一个优势是具有更好的功率峰均比。搭建了偏振复用CO-OFDM-OQAM系统的数值仿真平台，在背靠背(BtB)、100 km和200 km光纤传输3种场景下对所提方法的频谱效率、功率峰均比和信道估计性能进行了验证。获得的结果证实所提方法能够提高频谱效率，而且功率峰均比更加优良。

关键词 正交频分复用；偏振复用；信道估计；光通信系统

中图分类号 TN913.7 **文献标志码** A **DOI**：10.3788/AOS221761

1 引 言

随着通信技术的高速发展，多载波调制技术越来越受到人们的广泛重视。由于使用时频聚焦特性良好的脉冲成形滤波器，交错正交幅度调制的正交频分复用(OFDM-OQAM)系统具有更少的带外能量泄漏和更高的频谱效率[1-3]。相干光OFDM-OQAM系统与偏振复用方案(PDM CO-OFDM-OQAM)相结合可以进一步提升频谱效率和传输容量[4-6]。与传统OFDM系统不同，OFDM-OQAM系统只满足实数域正交性条件，不满足复数域正交性条件，产生了固有虚部干扰[7-8]，这种现象对OFDM-OQAM系统的信道估计过程有重要影响。特别是对于PDM CO-OFDM-OQAM系统[9]，不仅要考虑色散、噪声的影响，还要考虑固有虚部干扰和偏振模色散，信道估计算法的设计难度较高[10-11]。2013年，Horlin等[12]将OFDM-OQAM和PDM结合起来使用，频谱效率提高了1倍。同年，Li等[13]实验验证了PDM CO-OFDM-OQAM系统的有效性。然而，由于偏振模色散(PMD)和固有虚部干扰(IMI)的影响，PDM CO-OFDM-OQAM系统的信道均衡与其他偏振复用系统有很大区别[14-16]。Horlin等[12]为PDM CO-OFDM-OQAM系统设计了最小均方误差(MMSE)时域均衡器。Fang等[17]设计并研究了一种用于PDM CO-OFDM-OQAM系统的时域信道估计方法。Nhan等[18]重新设计了一种稀疏导频结构，利用它对PDM CO-OFDM-OQAM系统的信道响应进行估计。上述3种方法的共同问题是均为时域信道估计方案，具有高计算复杂度。计算复杂度较低的方法是在频域进行信道估计和均衡的。例如，Fang等[19]为PDM CO-OFDM-OQAM系统提出了两种频域信道估计方法，分别用半负载(half-loaded)导频和全负载(full-loaded)导频进行信道估计。在相同传输条件下，全负载型方法显示出更好的信道均衡特性。在文献[20]中，Lin等将两种方法应用于强度调制-直接检测的PDM OFDM-OQAM系统中。

从以上分析可知，PDM CO-OFDM-OQAM系统的信道估计方法分为两大类，第一类是时域方法，第二类是频域方法。时域方法计算复杂度很高，很难在实际环境中应用。频域方法包括两种：半负载(half-loaded)方法和全负载(full-loaded)方法。在相同传输条件下，全负载型方法显示出更好的信道均衡特性。传统的全负载方法使用基于实数导频的干扰近似训练序列(IAM-R)[19]或基于复数导频的增强型IAM(E-IAM-C)[18]。已经提出的频域信道估计方法面临2个问题：需要插入较多的零子载波形成保护间隔，频谱效率需要进一步提升；忽视了训练序列的功率峰均比

收稿日期：2022-09-27；**修回日期**：2022-10-30；**录用日期**：2023-02-27；**网络首发日期**：2023-03-09

基金项目：国家自然科学基金(62141505，61367007)、甘肃省自然科学基金(20JR10RA154)

通信作者：*cougarlz@lut.edu.cn

(PAPR)。本文设计了一种可用于PDM CO-OFDM-OQAM系统的高频谱效率频域信道估计方法，其特征在于：由训练序列和有效载荷组成数据帧，每个偏振分支的训练序列只需要4个频域符号，而其他频域估计方法至少需要6个频域符号，提高了频谱效率；实值导频是随机序列，不会使信号的功率峰均比变得更糟。为了验证所提方法的有效性，本文搭建了PDM CO-OFDM-OQAM系统的数值仿真平台，随后，研究了它在自发辐射(ASE)噪声信道和真实光纤信道中的信道估计性能。最后，对比了不同方法的信道估计和均衡能力。结果表明，即使对非线性光纤信道，所提方法仍具有很好的信道均衡性能。

2　PDM CO-OFDM-OQAM系统的调制和解调原理

图1是PDM CO-OFDM-OQAM系统的工作原理示意图，x偏振态和y偏振态上所传输的基带信号分别记为$s_x(t)$和$s_y(t)$，两者的数学表达式可以写为

$$\begin{cases} s_x(t)=\sum\limits_{n=1}^{N_s}\sum\limits_{m=0}^{M-1}a_{x,m,n}g(t-n\tau_0)\mathrm{e}^{\mathrm{j}2\pi mf_0\left(t-\frac{KM-1}{2}T_s\right)}\mathrm{e}^{\mathrm{j}\pi\frac{m+n-2mn}{2}} \\ s_y(t)=\sum\limits_{n=1}^{N_s}\sum\limits_{m=0}^{M-1}a_{y,m,n}g(t-n\tau_0)\mathrm{e}^{\mathrm{j}2\pi mf_0\left(t-\frac{KM-1}{2}T_s\right)}\mathrm{e}^{\mathrm{j}\pi\frac{m+n-2mn}{2}} \end{cases}, \tag{1}$$

式中：$g(t)$是脉冲成形滤波器；$a_{x,m,n}$和$a_{y,m,n}$代表在时频格点(m,n)处x和y偏振态传输的实值信号；M为子载波总数；相邻子载波间隔为$f_0=1/T$，T代表一个OFDM-OQAM复数符号的持续时间；T_s是时域采样间隔；K代表$g(t)$的重叠因子；N_s为每个偏振态上发送的实值符号的个数；τ_0是每个实值符号的持续时间。

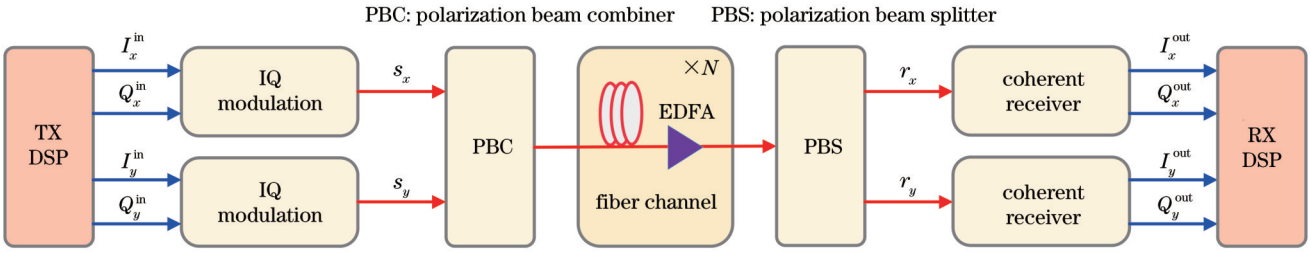

图1　PDM CO-OFDM-OQAM系统的工作原理示意图

Fig. 1　Schematic of the operating principle of the PDM CO-OFDM-OQAM system

时域波经过光纤信道时，会受到色散、偏振模色散及ASE噪声等的影响。使用h_{xx}、h_{yy}、h_{xy}和h_{yx}表示偏振复用光纤信道的信道脉冲响应，这里h_{xx}和h_{yy}分别是x偏振态和y偏振态上色散引起的脉冲响应，h_{xy}代表由PMD引起的x偏振态对y偏振态产生的偏振串扰，h_{yx}代表由PMD引起的y偏振态对x偏振态产生的偏振串扰。当光信号经过光纤信道后，接收端得到的接收信号为

$$\begin{bmatrix} r_x(t) \\ r_y(t) \end{bmatrix}=\begin{bmatrix} h_{xx} & h_{yx} \\ h_{xy} & h_{yy} \end{bmatrix}\otimes\begin{bmatrix} s_x(t) \\ s_y(t) \end{bmatrix}+\begin{bmatrix} w_x(t) \\ w_y(t) \end{bmatrix}, \tag{2}$$

式中：$w_x(t)$和$w_y(t)$是加性复数噪声，它们附加在x和y偏振态的传输信号中；符号$\otimes$表示矩阵元之间的卷积操作，即$r_{x/y}(t)=h_{xx/xy}\otimes s_x(t)+h_{yx/yy}\otimes s_y(t)+w_{x/y}(t)$。

接收信号经过光电转换后，还需要通过分析滤波器组(AFB)和快速傅里叶变换(FFT)来恢复子载波携带的数据。利用实数域的正交条件，可以得到(m,n)处的解调信号：

$$\begin{aligned} r_{x,m,n}=&H_{xx,m,n}a_{x,m,n}+\sum_{(p,q)\neq(0,0)}H_{xx,m+p,n+q}a_{x,m+p,n+q}\zeta_{m,n}^{m+p,n+q}+H_{yx,m,n}a_{y,m,n}+\\ &\sum_{(p,q)\neq(0,0)}H_{yx,m+p,n+q}a_{y,m+p,n+q}\zeta_{m,n}^{m+p,n+q}+W_{x,m,n}, \end{aligned} \tag{3}$$

$$\begin{aligned} r_{y,m,n}=&H_{yy,m,n}a_{y,m,n}+\sum_{(p,q)\neq(0,0)}H_{yy,m+p,n+q}a_{y,m+p,n+q}\zeta_{m,n}^{m+p,n+q}+H_{xy,m,n}a_{x,m,n}+\\ &\sum_{(p,q)\neq(0,0)}H_{xy,m+p,n+q}a_{x,m+p,n+q}\zeta_{m,n}^{m+p,n+q}+W_{y,m,n}, \end{aligned} \tag{4}$$

式中：$H_{xx,m,n}$、$H_{yy,m,n}$、$H_{xy,m,n}$和$H_{yx,m,n}$表示h_{xx}、h_{yy}、h_{xy}和h_{yx}的傅里叶变换结果，即信道频率响应；$\zeta_{m,n}^{m+p,n+q}=\left\langle g_{m,n},g_{m+p,n+q}\right\rangle=\int_{-\infty}^{+\infty}g_{m,n}(t)g_{m+p,n+q}^{*}(t)\mathrm{d}t$是固有虚

部干扰系数。光纤信道近似为慢时变信道，在一个符号持续时间内不同子载波对应的信道频率响应近似相等，则有以下关系成立：$H_{xx,m+p,n+q}\approx H_{xx,m,n}$、$H_{yy,m+p,n+q}\approx H_{yy,m,n}$、$H_{xy,m+p,n+q}\approx H_{xy,m,n}$和$H_{yx,m+p,n+q}\approx H_{yx,m,n}$。同时引入参数$a^{(\mathrm{i})}_{x,m,n}$和$a^{(\mathrm{i})}_{y,m,n}$，分别代表$x$和$y$偏振中邻近载波数据对时频格点$(m,n)$产生的固有虚部干扰，上角标(i)为固有虚部干扰标识，二者可写为

$$\begin{cases} a^{(\mathrm{i})}_{x,m,n}=\sum\limits_{(p,q)\in\Omega^{*}_{(1,1)}} a_{x,m+p,n+q}\left\langle g_{m,n},g_{m+p,n+q}\right\rangle \\ a^{(\mathrm{i})}_{y,m,n}=\sum\limits_{(p,q)\in\Omega^{*}_{(1,1)}} a_{y,m+p,n+q}\left\langle g_{m,n},g_{m+p,n+q}\right\rangle \end{cases}, \tag{5}$$

式中：$\Omega^{*}_{(1,1)}=\Omega_{(1,1)}-(0,0)$代表时频格点$(m,n)$的一阶最近邻区域。将式(5)代入式(3)和式(4)并改写为矩阵形式，可得

$$\begin{bmatrix} r_{x,m,n}\\ r_{y,m,n}\end{bmatrix}=\begin{bmatrix} H_{xx,m,n} & H_{yx,m,n}\\ H_{xy,m,n} & H_{yy,m,n}\end{bmatrix}\begin{bmatrix} a_{x,m,n}+a^{(\mathrm{i})}_{x,m,n}\\ a_{y,m,n}+a^{(\mathrm{i})}_{y,m,n}\end{bmatrix}+\begin{bmatrix} W_{x,m,n}\\ W_{y,m,n}\end{bmatrix}。 \tag{6}$$

由式(6)可知，为了得到每个子载波上的解调信息，可以执行如下操作：

$$\begin{bmatrix} \hat{a}_{x,m,n}\\ \hat{a}_{y,m,n}\end{bmatrix}=\mathrm{Re}\left\{\begin{bmatrix} h_{xx,m,n} & h_{yx,m,n}\\ h_{xy,m,n} & h_{yy,m,n}\end{bmatrix}^{-1}\begin{bmatrix} r_{x,m,n}\\ r_{y,m,n}\end{bmatrix}\right\}。 \tag{7}$$

3　高频谱效率的频域信道估计方法

为了进一步提升频谱效率，依据PDM CO-OFDM-OQAM系统的调制和解调原理，提出了一种具有高频谱效率、低PAPR的频域信道估计方法，其信号处理流程如图2所示。图3显示的是它使用的训练序列和帧结构。

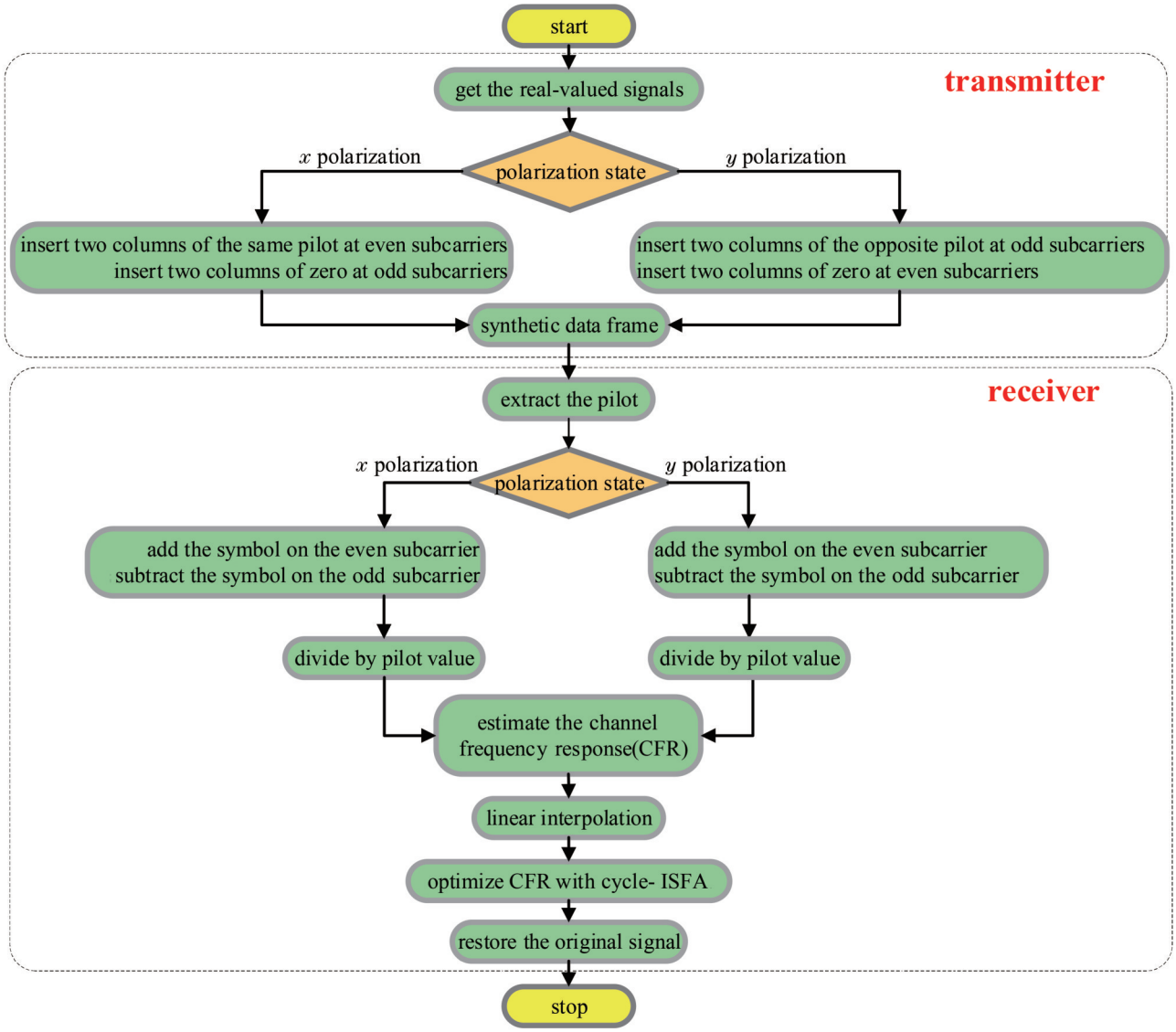

图2　所提方法的流程

Fig. 2　Flowchart of the proposed method

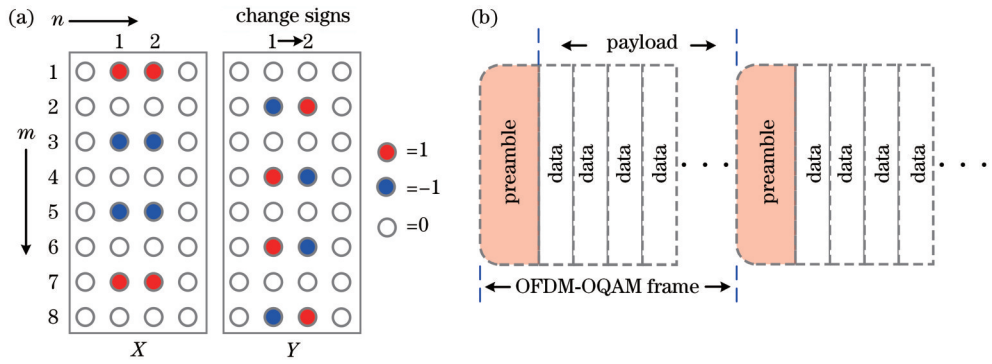

图 3　提出的两偏振态导频结构图。(a)训练序列;(b)帧结构

Fig. 3　Proposed pilot structure diagram of the dual-polarization states. (a) Training sequence; (b) frame structure

首先,在发射端训练序列和有效载荷组成数据帧,根据该数据帧生成基带发送信号。图 3(a)是所提方法的训练序列,x 偏振和 y 偏振的训练序列均占据 4 个频域符号,实值导频放置在第 2 和第 3 个频域符号。x 偏振的偶数子载波不为零,奇数子载波都为零;y 偏振的情况正好相反,奇数子载波不为零,偶数子载波都为零。实值导频前后各插入一个保护符号,两个偏振分支的帧结构如图 3(b)所示。为了方便起见,x 偏振方向的传送训练序列记作$\left[z, p_{x1}, p_{x2}, z\right]$,$y$ 偏振方向的传送序列记作$\left[z, p_{y1}, p_{y2}, z\right]$,它们满足

$$p_{x1,2m,n}\neq 0, p_{x1,2m+1,n}=0, p_{y1,2m,n}=0, p_{y1,2m+1,n}\neq 0, \tag{8}$$

$$p_{x1,2m,n}=p_{x2,2m,n}, p_{y1,2m+1,n}=-p_{y2,2m+1,n}。 \tag{9}$$

两个实值训练符号的时间位置用上角标(1)和(2)代表,则根据式(6)可得接收到的导频信号,表达式为

$$\begin{cases} r_{x,m,n}^{(1)}=H_{xx,m,n}\left(p_{x1,m,n}+p_{x1,m,n}^{(\mathrm{i})}\right)+H_{yx,m,n}\left(p_{y1,m,n}+p_{y1,m,n}^{(\mathrm{i})}\right)+w_x^{(1)} \\ r_{y,m,n}^{(1)}=H_{xy,m,n}\left(p_{x1,m,n}+p_{x1,m,n}^{(\mathrm{i})}\right)+H_{yy,m,n}\left(p_{y1,m,n}+p_{y1,m,n}^{(\mathrm{i})}\right)+w_y^{(1)} \end{cases}, \tag{10}$$

$$\begin{cases} r_{x,m,n}^{(2)}=H_{xx,m,n}\left(p_{x2,m,n}+p_{x2,m,n}^{(\mathrm{i})}\right)+H_{yx,m,n}\left(p_{y2,m,n}+p_{y2,m,n}^{(\mathrm{i})}\right)+w_x^{(2)} \\ r_{y,m,n}^{(2)}=H_{xy,m,n}\left(p_{x2,m,n}+p_{x2,m,n}^{(\mathrm{i})}\right)+H_{yy,m,n}\left(p_{y2,m,n}+p_{y2,m,n}^{(\mathrm{i})}\right)+w_y^{(2)} \end{cases}。 \tag{11}$$

如前文所述,导频 $p_{x1}, p_{x2}, p_{y1}, p_{y2}$ 满足式(8)和式(9),因此式(10)可以改写为

$$\begin{cases} r_{x,2m,n}^{(1)}=H_{xx,2m,n}\left(p_{x1,2m,n}+p_{x1,2m,n}^{(\mathrm{i})}\right)+H_{yx,m,n}\left(p_{y1,2m,n}^{(\mathrm{i})}\right) \\ r_{x,2m+1,n}^{(1)}=H_{xx,2m+1,n}\left(p_{x1,2m+1,n}^{(\mathrm{i})}\right)+H_{yx,2m+1,n}\left(p_{y1,2m+1,n}+p_{y1,2m,n}^{(\mathrm{i})}\right) \\ r_{y,2m,n}^{(1)}=H_{xy,2m,n}\left(p_{x1,2m,n}+p_{x1,2m,n}^{(\mathrm{i})}\right)+H_{yy,m,n}\left(p_{y1,2m,n}^{(\mathrm{i})}\right) \\ r_{y,2m+1,n}^{(1)}=H_{xy,2m+1,n}\left(p_{x1,2m+1,n}^{(\mathrm{i})}\right)+H_{yy,2m+1,n}\left(p_{y1,2m+1,n}+p_{y1,2m,n}^{(\mathrm{i})}\right) \end{cases}。 \tag{12}$$

同理,式(11)可以改写为

$$\begin{cases} r_{x,2m,n}^{(2)}=H_{xx,2m,n}\left(p_{x2,2m,n}+p_{x2,2m,n}^{(\mathrm{i})}\right)+H_{yx,m,n}\left(p_{y2,2m,n}^{(\mathrm{i})}\right) \\ r_{x,2m+1,n}^{(2)}=H_{xx,2m+1,n}\left(p_{x2,2m+1,n}^{(\mathrm{i})}\right)+H_{yx,2m+1,n}\left(p_{y2,2m+1,n}+p_{y2,2m,n}^{(\mathrm{i})}\right) \\ r_{y,2m,n}^{(2)}=H_{xy,2m,n}\left(p_{x2,2m,n}+p_{x2,2m,n}^{(\mathrm{i})}\right)+H_{yy,m,n}\left(p_{y2,2m,n}^{(\mathrm{i})}\right) \\ r_{y,2m+1,n}^{(2)}=H_{xy,2m+1,n}\left(p_{x2,2m+1,n}^{(\mathrm{i})}\right)+H_{yy,2m+1,n}\left(p_{y2,2m+1,n}+p_{y2,2m,n}^{(\mathrm{i})}\right) \end{cases}。 \tag{13}$$

根据 OFDM-OQAM 系统的调制和解调原理,可以证明具有固有虚部干扰系数 $\zeta_{m,n}^{m+p,n+q}$ 的图样具有对称性[21]:

$$\begin{bmatrix} \mathrm{j}(-1)^m\delta & -\mathrm{j}\beta & \mathrm{j}(-1)^m\delta \\ -\mathrm{j}(-1)^m\gamma & a_{m,n} & \mathrm{j}(-1)^m\gamma \\ \mathrm{j}(-1)^m\delta & \mathrm{j}\beta & \mathrm{j}(-1)^m\delta \end{bmatrix}。 \tag{14}$$

如前所述,实值导频满足 $p_{x1,2m,n}=p_{x2,2m,n}, p_{y1,2m+1,n}=-p_{y2,2m+1,n}$。根据式(9)和式(14)的对称性,可以证明实值导频的虚部干扰满足

$$p_{x1,2m,n}^{(\mathrm{i})}=-p_{x2,2m,n}^{(\mathrm{i})}, p_{x1,2m+1,n}^{(\mathrm{i})}=p_{x2,2m+1}^{(\mathrm{i})}, \tag{15}$$

$$p_{y1,2m,n}^{(\mathrm{i})}=-p_{y2,2m,n}^{(\mathrm{i})}, p_{y1,2m+1,n}^{(\mathrm{i})}=-p_{y2,2m+1}^{(\mathrm{i})}。 \tag{16}$$

将式(15)和式(16)分别代入式(12)和式(13)中,经过计算,可得

$$r_{x,2m,n}^{(1)}+r_{x,2m,n}^{(2)}=H_{xx,2m,n}2p_{x1,2m,n}, \tag{17}$$

$$r_{x,2m+1,n}^{(1)}-r_{x,2m+1,n}^{(2)}=H_{yx,2m+1,n}2p_{y1,2m+1,n}, \tag{18}$$

$$r^{(1)}_{y,2m,n}+r^{(2)}_{y,2m,n}=H_{xy,2m,n}2p_{x1,2m,n}, \tag{19}$$

$$r^{(1)}_{y,2m+1,n}-r^{(2)}_{y,2m+1,n}=H_{yy,2m+1,n}2p_{y1,2m+1,n}。 \tag{20}$$

从式(17)～(20)可以看出，信道频率响应系数的估算公式为

$$\begin{cases} H_{xx,2m,n}=\dfrac{r^{(1)}_{x,2m,n}+r^{(2)}_{x,2m,n}}{2p_{x1,2m,n}} \\ H_{yx,2m+1,n}=\dfrac{r^{(1)}_{x,2m+1,n}-r^{(2)}_{x,2m+1,n}}{2p_{y1,2m+1,n}} \\ H_{xy,2m,n}=\dfrac{r^{(1)}_{y,2m,n}+r^{(2)}_{y,2m,n}}{2p_{x1,2m,n}} \\ H_{yy,2m+1,n}=\dfrac{r^{(1)}_{y,2m+1,n}-r^{(2)}_{y,2m+1,n}}{2p_{y1,2m+1,n}} \end{cases}, \tag{21}$$

其他偶数和奇数子载波位置的信道响应系数则可以利用插值法计算得到。

最后，为了抵抗噪声和干扰的影响，利用符号内频域平均(ISFA)进一步提升信道估计精度，即每个频率点的ISFA信道估计值等于该点之前k个点和该点之后k个点的平均值。ISFA之后的信道频率响应可以表示为

$$\left[h^{\mathrm{ML}}_{m'}\right]_{\mathrm{ISFA}}=\frac{\sum_{m=m'-k}^{m'+k}\left[h^{\mathrm{ML}}_{m}\right]}{\min(m_{\max},m'+k)-\max(m_{\min},m'-k)+1}, \tag{22}$$

式中：$\left[h^{\mathrm{ML}}_{m}\right]$为第$m$个子载波的最小二乘信道估计值；$m_{\max}$和$m_{\min}$是有效子载波数的最大值和最小值。对信道估计值重复进行ISFA，经过多次循环后，进一步提高了信道估计精度。优化信道频率响应完成后，再利用式(7)所示的操作恢复出全部有效载荷的原始信息。

4　结果分析与讨论

为了验证所提方法的信道估计能力，搭建了CO-OFDM-OQAM通信系统的数值仿真平台，具体配置如图4所示。该系统的时域采样速率设定为20 GSa/s。子载波总数(傅里叶变换点数)为512，调制格式均为16-QAM，激光器的中心频率为193.4 THz。在发送端，首先生成在x和y偏振态上传输的二进制比特序列，分别经Offset-QAM调制、快速傅里叶逆变换、综合滤波器组后，生成两路电信号。在发射端，激光器发出的光源经过偏振分束器产生两路偏振正交的光束，两路光在马赫-曾德尔调制器中分别与x、y路电信号进行光载波调制，形成携带数据信息的x和y偏振态光信号。然后，由偏振合束器将两路信号光合并到一起，经光纤链路进行传输。在接收端，首先接收到的光信号经过偏振分束器分解成x和y两路光信号，与本振激光器发出的光束进行混频后，进入平衡探测器生成两路电信号。电域数字信号处理包括滤波器组分析、傅里叶变换、Offset-QAM解调、信道响应估计和均衡，最后得到两支路所传输的二进制比特序列，并统计误码率。本文以耦合非线性薛定谔方程为基础建立偏振复用光纤信道的模型，通过分步傅里叶算法求解耦合非线性薛定谔方程来模拟标准单模光纤(SSMF)中光信号的传输过程。如果将耦合非线性薛定谔方程的非线性折射率设定为零，则信道为线性光纤信道，反之为非线性光纤信道。

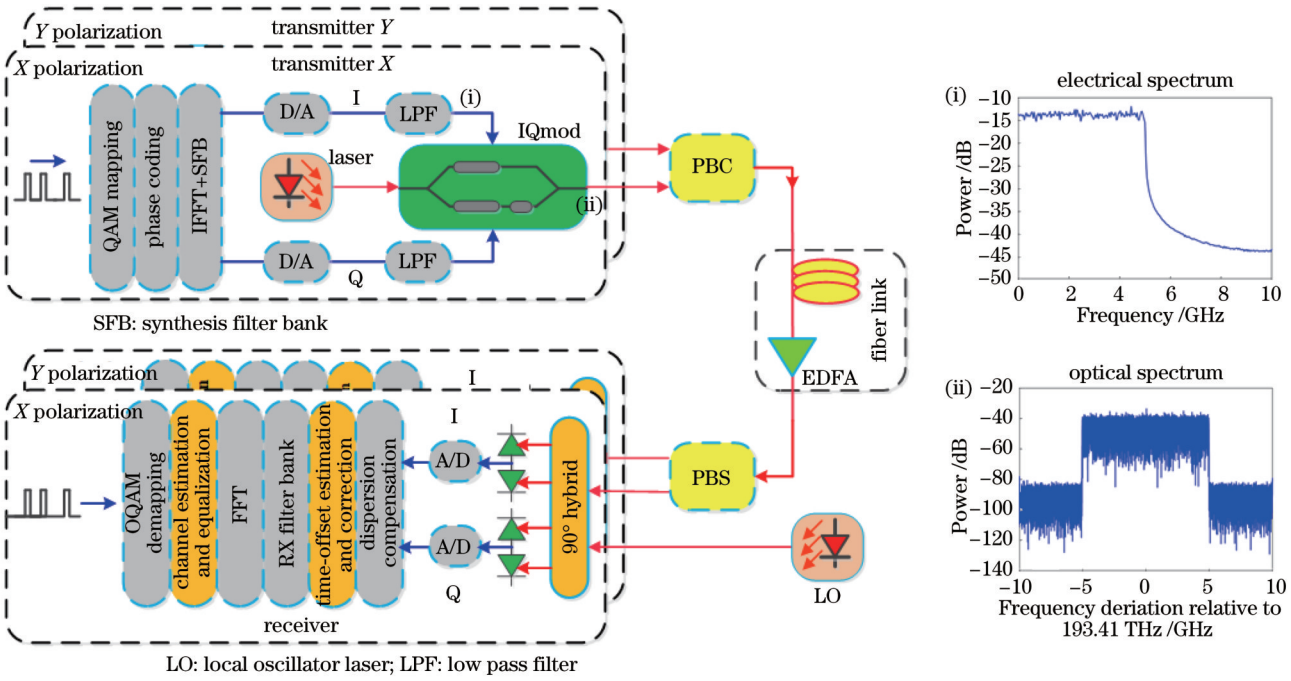

图4　PDM CO-OFDM-OQAM系统的数值仿真配置，插图显示了它的电谱和光谱

Fig. 4　Simulation configuration of the PDM CO-OFDM-OQAM system, the insets show its electrical and optical spectra

首先，计算使用不同信道估计方法时 PDM CO-OFDM-OQAM 系统的 PAPR 值。这些 PAPR 值是测量时域样本的峰值功率与平均功率之比得到的，形式为

$$R_{\mathrm{PAPR}}=10\log_{10}\frac{\max\left[|s(t)|^2\right]}{E\left[|s(t)|^2\right]},\tag{23}$$

式中：$s(t)$是传输信号在时间上的采样点；$E[\cdot]$表示期望算子。由于 PAPR 在 OFDM-OQAM 符号之间随机变化，对多载波信号来说，更好的衡量标准是互补累积分布函数（CCDF），即 PAPR 超过给定阈值的概率。如果阈值表示为 T_{h}，那么 CCDF 可以表示为 $F_{\mathrm{CCDF}}=1-\mathrm{Prob}(R_{\mathrm{PAPR}}\leqslant T_{\mathrm{h}})$。对 x 和 y 偏振态进行平均后获得的结果如图 5 所示。该图清楚地显示了插入训练序列前后系统 PAPR 性能的变化。从图 5 可以发现：E-IAM-C 对系统 PAPR 性能的影响是最大的，而所提方法影响最小；IAM-R 方法对系统的影响几乎与半负载型方法相同。图 5 还显示了每种方法的训练序列需要占用的频域符号数。IAM-R 方法和半负载型方法的每个偏振分支上训练序列需要占用 6 个频域符号，E-IAM-C 方法需要占用 8 个频域符号，而所提方法只需要占用 4 个频域符号。

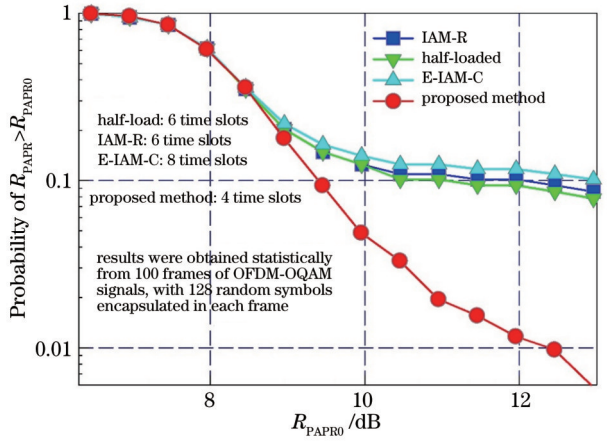

图 5　PDM CO-OFDM-OQAM 系统下，使用互补累积分布函数表示不同信道估计方法的 PAPR 性能

Fig. 5　PAPR performance of different channel estimation methods represented using complementary cumulative distribution function under the PDM CO-OFDM-OQAM system

接下来，研究背靠背情况下所提方法的信道估计性能，结果如图 6 所示。图 6 显示了系统误码率和光信噪比（OSNR）之间的对应关系，可以看出：在光背靠背情况下，当 OSNR 小于 23 dB 时，经过 6 次 ISFA 循环后所提方法的误码率优于 IAM-R 方法；当 OSNR 小于 27 dB 时，经过 8 次 ISFA 循环后所提方法的误码率都优于 IAM-R 方法；在所考察的整个 OSNR 范围内（10 dB～30 dB），经过 10 次 ISFA 循环后，所提方法的误码率始终优于 IAM-R 方法。

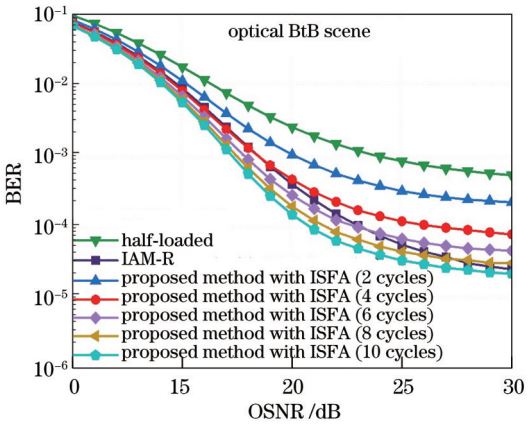

图 6　光背靠背情况下不同信道估计方法的误码率性能

Fig. 6　BER performance of different channel estimation methods in optical BtB scene

经过 100 km 和 200 km SSMF 传输后所提方法的信道估计性能如图 7 所示。在做这项研究时，暂时没有考虑光纤非线性，光纤色散系数取 16 ps·nm^{-1}·km^{-1}，差分群延迟（DGD）设定为 5 ps·km$^{-1/2}$。在 100 km 光纤传输情况下，当 OSNR 小于 23 dB 时，经过 6 次 ISFA 循环后，所提方法的误码率优于 IAM-R 方法；在 12 dB～25 dB 的 OSNR 范围内，经过 8 次 ISFA 循环后，所提方法的误码率始终优于 IAM-R 方法。如果光纤长度增大至 200 km，则当 OSNR 小于 21.5 dB 时，所提方法经过 6 次 ISFA 循环后的误码率优于 IAM-R 方法；当 OSNR 小于 22.5 dB 时，经过 8 次 ISFA 循环后所提方法的误码率始终优于 IAM-R 方法。本文将光纤的 DGD 设定为较大的值，而标准单模光纤的 DGD 通常小于 0.5 ps·km$^{-1/2}$。DGD 值越大，PMD 引起的偏振串扰越严重。因此，图 7 结果充分说明所提方法在 PMD 影响较严重的情况下仍然具有良好的信道估计能力。

光纤信道和无线信道之间的一个重要区别是光纤存在非线性，这会导致自相位调制、交叉相位调制、四波混频等物理损伤。然而，文献[17-19]并没有考虑光纤非线性。在上一阶段的研究中，本文对比了不同方法在线性光纤信道中的信道估计能力，暂时忽略了光纤的非线性。本文的最后部分重点研究所提方法在非线性光纤信道中的信道估计性能。图 8 显示了 100 km SSMF 传输后 BER 与光纤输入功率的对应关系。光纤非线性造成的损伤由非线性折射率（2.6×10^{-20} m^2/W）来描述。EDFA 引入 ASE 噪声，它的噪声指数为 4 dB。DGD 仍设定为 5 ps·km$^{-1/2}$。7% 硬判决前向纠错码（FEC）极限在图 8 中用虚线标出。非线性光纤信道产生两个噪声源：ASE 噪声和非线性干扰。如图 8 所示：当入纤功率较小时，接收信号质量主要受 ASE 噪声的限制；随着入纤功率逐渐增大，信噪比越来越高，因此 BER 逐渐减小；在最佳输入功率下，BER

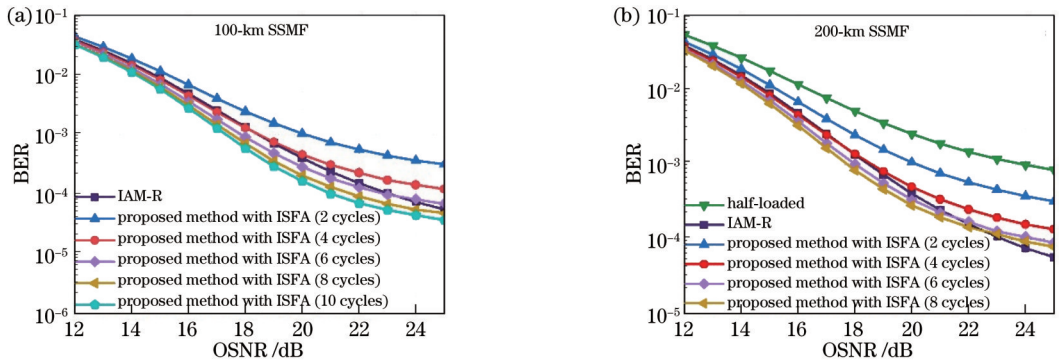

图 7　SSMF 传输后不同信道估计方法的误码率性能。(a) 100 km 传输；(b) 200 km 传输

Fig. 7　BER performance of different channel estimation methods under SSMF transmission. (a) 100-km SSMF transmission; (b) 200-km SSMF transmission

取最小值；当入纤功率继续增加，非线性干扰开始占主导地位，并严重降低接收信号质量，此时入纤功率越大，则非线性干扰越强，BER 性能下降得越厉害。当入纤功率取给定值时，从图 8 可以看出，随着 ISFA 循环次数从 1 增加至 3，所提方法所对应的 BER 逐渐减小，信号传输质量逐渐提升，3 种情况对应的优化输入功率分别为 −2 dBm、−3 dBm 和 −1 dBm。以上结果充分表明，所提方法在线性和非线性光纤信道中均能够提供足够好的信道估计能力。

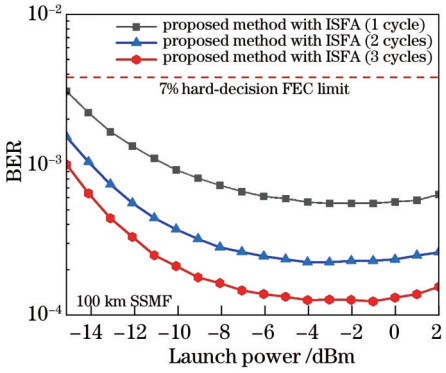

图 8　非线性光纤信道中所提方法的误码率性能

Fig. 8　BER performance of the proposed method in a nonlinear fiber channel

5　结　　论

为 PDM CO-OFDM-OQAM 系统提出并研究了一种改进的频域信道估计方法。该方法的主要优点是每个偏振分支的训练序列只需要 4 个频域符号。相比 IAM-R 方法，训练序列所占符号数降低了 33.3%，相比 E-IAM-C 方法，训练序列所占符号数降低了 50%，明显提升了频谱效率。另一个明显优势是实值导频选取为随机序列，避免不同信号成分之间发生相长干涉，功率峰均比性能更加优良。在实际光纤信道中对所提方法的信道估计能力进行了数值验证，考虑了光纤色散、偏振模色散和非线性的影响。结果发现，即使对于非线性光纤信道，所提方法也能获得较好的 BER 性能。所提方法能够为研发基于 OFDM-OQAM 的短途光纤通信系统提供有益参考。

参　考　文　献

[1] Nissel R, Schwarz S, Rupp M. Filter bank multicarrier modulation schemes for future mobile communications[J]. IEEE Journal on Selected Areas in Communications, 2017, 35(8): 1768-1782.

[2] Shieh W, Yang Q, Ma Y. 107 Gb/s coherent optical OFDM transmission over 1000-km SSMF fiber using orthogonal band multiplexing[J]. Optics Express, 2008, 16(9): 6378-6386.

[3] Haider F. Cellular architecture and key technologies for 5G wireless communication networks[J]. Journal of Chongqing University of Posts & Telecommunications, 2014, 52(2): 122-130.

[4] Siohan P, Siclet C, Lacaille N. Analysis and design of OFDM/OQAM systems based on filterbank theory[J]. IEEE Transactions on Signal Processing, 2002, 50(5): 1170 - 1183.

[5] Nedic S. An approach to data-driven echo cancellation in OQAM-based multicarrier data transmission[J]. IEEE Transactions on Communications, 2000, 48(7): 1077-1082.

[6] Le Floch B, Alard M, Berrou C. Coded orthogonal frequency division multiplex[TV broadcasting] [J]. Proceedings of the IEEE, 1995, 83(6): 982-996.

[7] 刘俊杰，王道斌，拓明珊，等. 相干光FBMC-OQAM系统的时间偏移和信道联合估计算法[J]. 中国激光，2020，47(11)：1106001.
Liu J J, Wang D B, Tuo M S, et al. Joint estimation algorithm of time offset and channel response for coherent optical FBMC-OQAM systems[J]. Chinese Journal of Lasers, 2020, 47(11): 1106001.

[8] 崇涵丹，王道斌，元丽华，等. 相干光FBMC/OQAM系统的整数频偏估计与补偿方法[J]. 光学学报，2019，39(12)：1206008.
Chong H D, Wang D B, Yuan L H, et al. Estimation and compensation of integer frequency offset in coherent optical offset quadrature amplitude modulation based filter bank multicarrier systems[J]. Acta Optica Sinica, 2019, 39(12): 1206008.

[9] Yeh C H, Hsu W H, Wang B Y, et al. Dual-polarized WDM access network with fiber to the extension (FTTE) connection [J]. IEEE Photonics Journal, 2021, 13(4): 7200106.

[10] Ibragimov E, Schmidt T J. Polarization monitoring in polarization division multiplexing in optical communications: US08032025B2[P]. 2011-10-04.

[11] Shieh W, Yi X, Ma Y, et al. Theoretical and experimental

study on PMD-supported transmission using polarization diversity in coherent optical OFDM systems[J]. Optics Express, 2007, 15(16): 9936-9947.
[12] Horlin F, Fickers J, Emplit P, et al. Dual-polarization OFDM-OQAM for communications over optical fibers with coherent detection[J]. Optics Express, 2013, 21(5): 6409-6421.
[13] Li Z H, Jiang T, Li H B, et al. Experimental demonstration of 110-Gb/s unsynchronized band-multiplexed superchannel coherent optical OFDM/OQAM system[J]. Optics Express, 2013, 21(19): 21924-21931.
[14] Yao X S, Yan L S, Zhang B, et al. All-optic scheme for automatic polarization division demultiplexing[J]. Optics Express, 2007, 15(12): 7407-7414.
[15] Stuart H R. Dispersive multiplexing in multimode fiber[J]. Science, 2000, 289(5477): 281.
[16] Cheng Y, Tan J, Liu L, et al. Method of joint frame synchronization and data-aided channel estimation for 100-Gb/s polarization-division multiplexing - single carrier frequency domain equalization coherent optical transmission systems[J]. Optical Engineering, 2016, 55(2): 026118.
[17] Fang X, Xu Y C, Chen Z Y, et al. Time-domain least square channel estimation for polarization-division-multiplexed CO-OFDM/OQAM systems[J]. Journal of Lightwave Technology, 2016, 34(3): 891-900.
[18] Nhan N Q, Morel P, Azou S, et al. Sparse preamble design for polarization division multiplexed CO-OFDM/OQAM channel estimation[J]. Journal of Lightwave Technology, 2018, 36(13): 2737-2745.
[19] Fang X, Xu Y C, Chen Z Y, et al. Frequency-domain channel estimation for polarization-division-multiplexed CO-OFDM/OQAM systems[J]. Journal of Lightwave Technology, 2015, 33(13): 2743-2750.
[20] Lin B J, Fang X, Tang X, et al. Efficient frequency-domain channel equalization methods for dual-polarization orthogonal frequency-division multiplexing/offset quadrature amplitude modulation-passive optical network[J]. Optical Engineering, 2016, 55(10): 106108.
[21] Kofidis E, Katselis D, Rontogiannis A, et al. Preamble-based channel estimation in OFDM/OQAM systems: a review[J]. Signal Processing, 2013, 93(7): 2038-2054.

Frequency-Domain Channel Estimation for Polarization-Division-Multiplexed CO-OFDM-OQAM Systems with High Spectrum Efficiency

Zhang Shuo, Wang Daobin*, Zhao Hangyu, Huang Quansheng, Song Tingting, Yuan Lihua
School of Science, Lanzhou University of Technology, Lanzhou 730050, *Gansu, China*

Abstract

Objective OFDM-OQAM involves special modulation and demodulation methods, owing to which offers several advantages, including flexible time-frequency lattice, very low out-of-band spectral leakage, and excellent spectral efficiency. Presently, it is widely applied in fields such as wireless communication and optic-fiber communication. In the past, several frequency-domain channel estimation methods have been proposed for CO-OFDM-OQAM. However, these methods are associated with various drawbacks. For instance, more guard intervals need to be inserted between the training sequence and payload to reduce the influence of inherent imaginary part interference (IMI), which can lead to excessive spectrum resources. Thus, this work proposes and studies an improved frequency-domain channel estimation method for PDM CO-OFDM-OQAM systems. The proposed method remarkably enhances the spectrum efficiency and does not severely degrade the power peak-to-average ratio (PAPR) of the signal.

Methods A fully-loaded training sequence was designed using real-valued pilots based on the demodulation principle of a polarization multiplexing system and the symmetry rules of an inherent imaginary interference. This method was combined with the interpolation method to ensure that number of frequency-domain symbols to be occupied by the training sequence on each polarization state was reduced to four. The training sequence and the payload at the transmitter's end form a data frame, which assist in generating a baseband transmission signal. The training sequences of x-polarized and y-polarized states occupied four frequency-domain symbols and the real-valued pilots were placed in the 2nd and 3rd frequency-domain symbols. All the odd-numbered subcarriers of the x-polarized state were zero, while the even-numbered subcarriers were not zero. In contrast, the odd-numbered subcarriers of the y-polarized state were not zero, while all the even-numbered subcarriers were zero. For convenience, we denoted the transmission training sequences in the x- and y- polarized directions as $[z, p_{x1}, p_{x2}, z]$ and $[z, p_{y1}, p_{y2}, z]$, respectively. These transmission sequences satisfy the given symmetry conditions. The channel frequency response coefficients at the receiver's end for a portion of the subcarriers were estimated using the analytical formula. Alternatively, the channel response coefficients for other even and odd subcarrier positions were calculated using the interpolation method. Finally, intra-symbol frequency-domain average (ISFA) was used to lessen the influence of noise and interference and to further improve the channel estimation accuracy. In addition, the PAPR values of PDM CO-OFDM-OQAM were calculated using different channel estimation methods.

Results and Discussions In this paper, a numerical simulator for a polarization multiplexing CO-OFDM-OQAM system is developed. By using the simulator, the spectral efficiency, peak-to-average power ratio, and channel estimation performance of the method have been verified under three scenes of back-to-back (BtB), 100-km, and 200-km fiber transmissions. Our findings reveal that E-IAM-C method has the greatest impact on the PAPR performance of the system, while the proposed method has the least impact. Furthermore, the investigation of channel estimation performance of the proposed method in the BtB case reveals that the BER of the proposed method after 10 cycles of ISFA shows better results than that of the interference approximation method using real-valued pilots (IAM-R) in the OSNR range under investigation (10 dB-30 dB). This work also focuses on the channel estimation performance of the proposed method in nonlinear fiber channels. Overall, our results demonstrate that the proposed method provides an efficient channel estimation capability in both linear and nonlinear fiber channels.

Conclusions This work proposes and studies an improved frequency-domain channel estimation method for PDM CO-OFDM-OQAM systems. The main advantage of this method is that it only requires four frequency-domain symbols for the training sequence of each polarization branch. Compared with IAM-R and the E-IAM-C method that uses complex pilots, number of symbols occupied by the training sequence of the proposed method is reduced by 33.3% and 50%, respectively. Thus, the proposed method substantially improves spectral efficiency. In addition, in the proposed method, the real-valued pilot is a random sequence, which does not worsen the PAPR of the signal. The channel estimation capability of the proposed method is verified quantitively in an actual fiber channel by considering the effects of fiber dispersion, polarization mode dispersion, and nonlinearity. Moreover, the results show that the proposed method achieves better BER performance even for nonlinear fiber channels. The findings of this work provide useful insights into the research and development of short-distance fiber communication systems based on OFDM-OQAM.

Key words orthogonal frequency division multiplexing; polarization-division-multiplexing; channel estimation; optical communication system